# Supporting Information

**Electrochemically Reconstructing of 1D Cu(PyDC)(H$_2$O) MOF into In-situ Formed Cu-Cu$_2$O Heterostructures on Carbon Cloth as Efficient Electrocatalyst for CO$_2$ Conversion**

Manjunatha Kempasiddaiah,[a,b] Rajib Samanta,[a,b] Sonali Panigrahy,[a,b] Ravi Kumar Trivedi,[c,d] Brahmananda Chakraborty,*[b,e] and Sudip Barman*[a,b]

[a]School of Chemical Sciences, National Institute of Science Education and Research (NISER), Bhubaneswar-752050, Orissa, India.

[b]Homi Bhabha National Institute, Training School Complex, Anushakti Nagar, Mumbai - 400094, India.

[c]Department of Physics, Karpagam Academy of Higher Education, Coimbatore 641021, Tamil Nadu, India.

[d]Centre for Computational Physics, Karpagam Academy of Higher Education, Coimbatore 641021, Tamil Nadu, India.

[e]High Pressure & Synchroton Radiation Physics Division, Bhabha Atomic Research Centre, Trombay, Mumbai-400085, India.

**E-mail:** sbarman@niser.ac.in
          brahma@barc.gov.in

## Table of Contents

## 1. Chemicals and Materials

Copper (II) nitrate trihydrate ($Cu(NO_3)_2 \cdot 3H_2O$), 2,5-Pyridinedicarboxylic acid (2,5-$H_2$PyDC), *N,N*-dimethylformamide (DMF), Nafion D-520 dispersion (5 wt% in isopropyl alcohol and water), Potassium hydrogen carbonate ($KHCO_3$) were purchased from Sigma-Aldrich, Alfa Aesar and TCI chemical companies. Deuterium oxide ($D_2O$) was obtained from Fisher Scientific chemical companies. Unless otherwise specified, all chemicals and reagents are of analytical grade and have been used as such without additional purifications. Toray carbon cloth (TGP-H-60) and Nafion 117 proton exchange membrane were purchased from Alfa Aesar and Sigma Aldrich, respectively. A high-purity $CO_2$ (99.999%), $N_2$ (99.998%), $H_2$ (99.999%) and Ar (99.998%) were received from Sigma Aldrich.

## 2. Instrumentation and Analyses

The crystallographic information of Cu-MOF was collected from the Rigaku XtaLab SuperNova diffractometer equipped with Cu Kα radiation ($\lambda = 1.54184$ Å) at 210(4) K. Surface morphology was analyzed using field-emission scanning electron microscope (FE-SEM) (Carl Zeiss, Germany, Model: ∑igma). Samples for FE-SEM analysis were prepared by drop casting 0.05 mL of solution (1 mg/mL) on silicon wafer and dried at 45 °C in air atmosphere. The surface morphology was further investigated by high-resolution transmission electron microscopy (HRTEM, JEOL F200) at 200 kV. For TEM analysis, a 10 µL solution of 1 mg/mL stock solution was drop-costed on TEM grid and dried at 45 °C in air. Bruker DAVINCI D8 ADVANCE diffractometer equipped with Cu Kα radiation ($\lambda = 0.15406$ nm) was used to obtain X-ray diffraction patterns (*p*-XRD). VG Microtech was used to perform x-ray photoelectron spectroscopy measurements by drop-casting the samples on silicon wafers, and the monochromatic source was Mg K X-ray. Total metal content loading was quantified by

ThemoScientific's iCAP 7000 series inductively coupled plasma-optical emission spectroscopy (ICP-OES). PGSTAT 320N electrochemical workstation (Autolab, Metrohm) was used to perform all the electrochemical measurements. A pH meter Hanna (HI 2209) was used to measure the pH of the working electrolyte. An ultrasound bath sonication was conducted by using Genei Laboratories Private Limited, Bangalore, India. In this study, $^1$H NMR spectra were recorded by Bruker 400 MHz NMR system through water suppression method.

## 3. Synthesis of Catalysts

### 3.1. Hydrothermal preparation of 1D Cu(PyDC)(H$_2$O) MOF

In a typical synthesis procedure, 1 mmol of 2,5-H$_2$PyDC (2,5-pyridinedicarboxylic acid) was magnetically stirred in deionized water (25 mL) for 1 hour at ambient temperature. A blue solution was attained after the addition of 1 mmol of Cu(NO$_3$)$_2$·3H$_2$O (copper (II) nitrate trihydrate), which was further stirred for additional 30 minutes. The resulting blue-suspension was sealed in a Teflon-lined stainless-steel autoclave and kept inside the hot-air oven and heated at 160 °C for 72 hours. After the reaction completion, autoclave was allowed to room temperature, a blue-colored crystals of Cu(PyDC)(H$_2$O), suitable for X-ray crystallography, were obtained at the bottom of the autoclave. Finally, the crystals were washed with DMF and deionized H$_2$O twice (2 x 10 mL), dried at 80 °C (yield: 85 % based on Cu). Anal. Calcd for C$_7$H$_5$NO$_5$Cu: (M$_r$ = 246.66): C, 34.08; H, 2.04; N, 5.68. Found: C, 33.89; H, 2.06; N, 5.52 %. IR spectrum (cm$^{-1}$): 2778, 1682, 1614, 1534, 1408, 1166, 1042, 828, 761.

### 3.2. Preparation of Cu-Cu$_2$O/NC composites

The Cu-Cu$_2$O/NC electrocatalysts were prepared through carbonizing as such prepared Cu(PyDC)(H$_2$O) crystals at different temperatures of 600, 700 and 800 °C for 2 hours under ultrahigh-purity N$_2$ atmosphere with a heating rate of 2 °C/min and were named as Cu-Cu$_2$O/NC-600, Cu-Cu$_2$O/NC-700 and Cu-Cu$_2$O/NC-800, respectively.

**4. Table S1.** Crystal data and structure refinement details for $Cu(PyDC)(H_2O)$:

| Empirical formula | $C_7H_5CuNO_5$ |
|---|---|
| Formula weight (g/mol) | 246.66 |
| Crystal system | Orthorhombic |
| Space group | Pccn |
| Temperature/K | 210(4) |
| a (Å) | 20.4886(5) |
| b (Å) | 11.6812(3) |
| c (Å) | 6.3843(10) |
| $\alpha/°$ | 90 |
| $\beta/°$ | 90 |
| $\gamma/°$ | 90 |
| V (Å3) | 1527.96(6) |
| Z | 8 |
| $\rho_c$ (g/cm$^3$) | 2.144 |
| Crystal size (mm) | 0.30 x 0.28 x 0.25 |
| Crystal type | Blue block |
| $\mu/mm^{-1}$ | 4.082 |
| F000 | 984.0 |
| Reflections collected | 6766 |
| Independent reflections | 1573 [$R_{int} = 0.0286$, $R_{sigma} = 0.0221$] |
| data/restraints/parameters | 1573/4/134 |
| Goodness-of-fit on $F^2$ | 1.071 |
| Final $R$ indices [$I > 2\sigma(I)$] | $R_1 = 0.0252$, w$R_2 = 0.0714$ |
| Final $R$ indices (all data) | $R_1 = 0.0265$, w$R_2 = 0.0726$ |

**5. Figure S1:** (a-f) STEM and corresponding elemental mapping of Cu(PyDC)(H$_2$O) MOF.
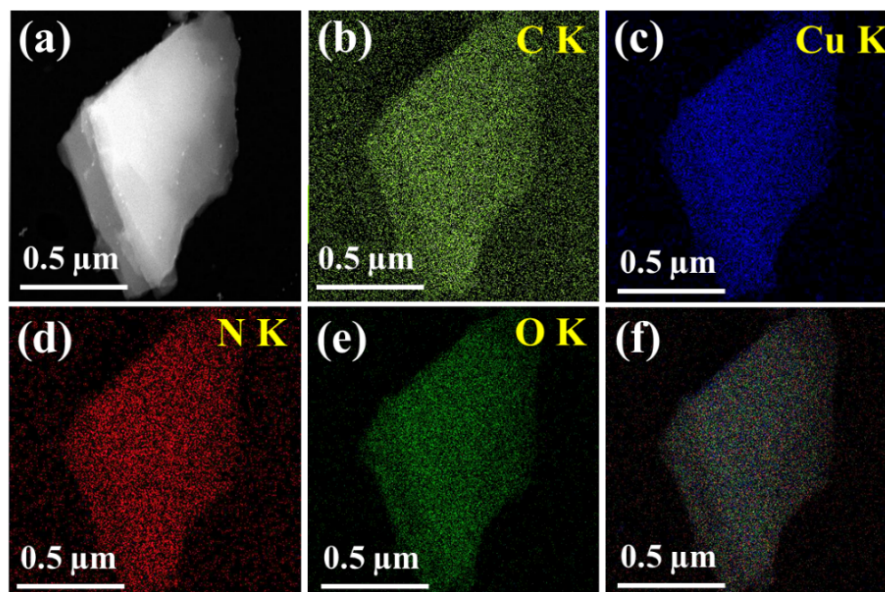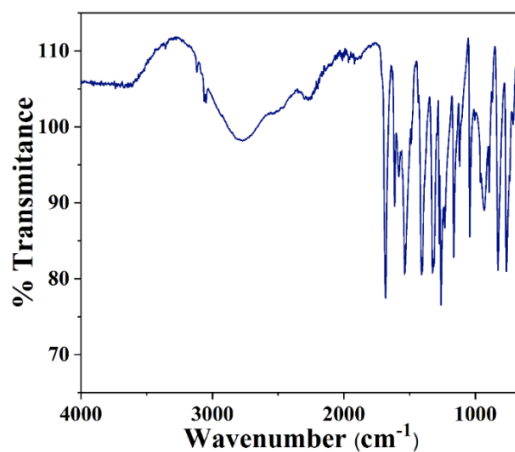


**6. Figure S2:** (a-c) high-resolution XPS spectra of C 1s, O 1s and N 1s of 1D Cu(PyDC)(H$_2$O) MOF, respectively.
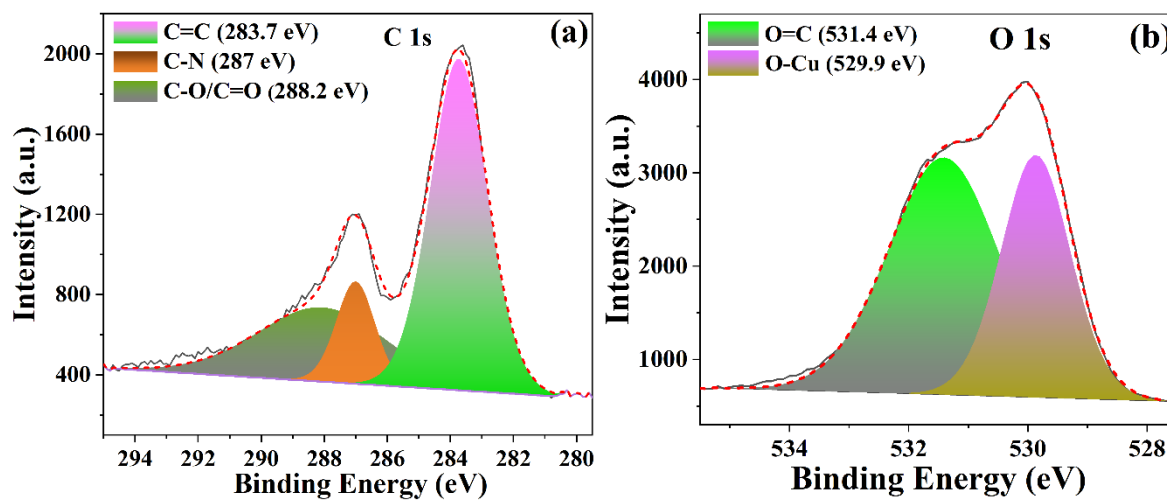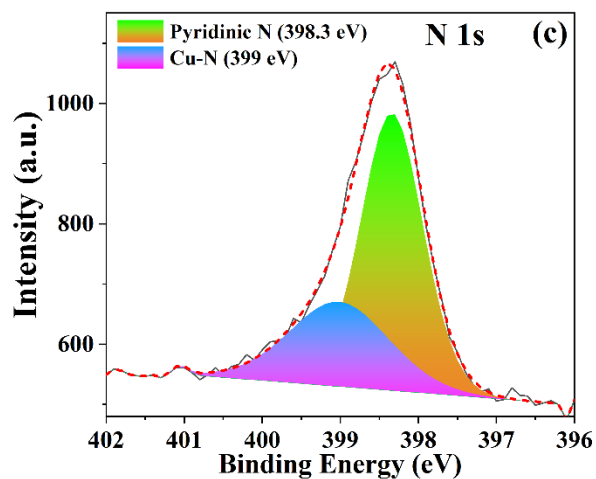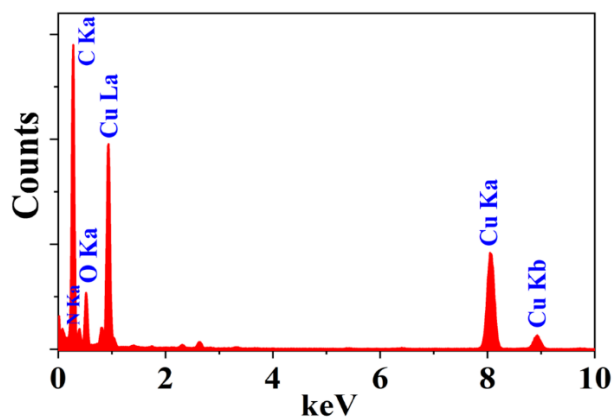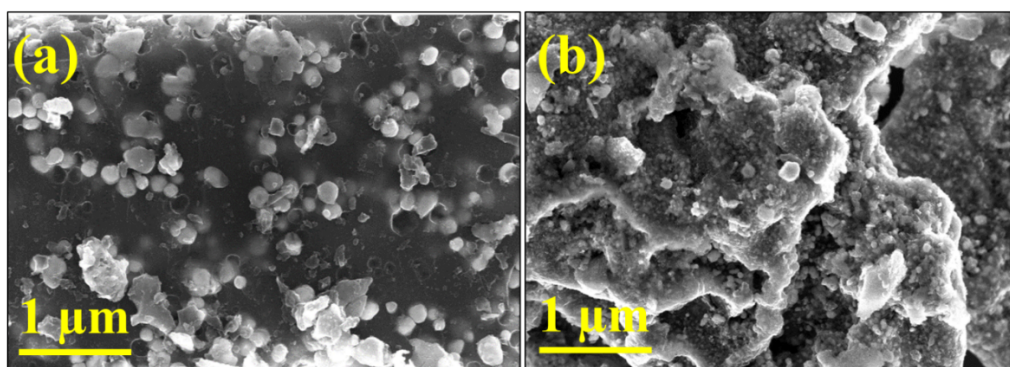
**7. Figure S3.** ATR-IR spectra of Cu(PyDC)(H$_2$O) MOF.



**8. Figure S4.** EDS spectrum of Cu-Cu$_2$O/NC-700 composite.



**9. Figure S5.** SEM images of Cu-Cu$_2$O/NC-600 & Cu-Cu$_2$O/NC-800 composites.

**10. Table S2.** CHNS analysis of Cu-Cu$_2$O/NC composites.

| Composites (Element %) | C | N | H |
|---|---|---|---|
| Cu-Cu$_2$O/NC-600 | 32.07 | 7.52 | 0.70 |
| Cu-Cu$_2$O/NC-700 | 31.85 | 5.93 | 0.50 |
| Cu-Cu$_2$O/NC-800 | 28.81 | 5.14 | 0.32 |

**11. Figure S6.** X-ray photoelectron spectroscopy (a) survey spectra and (b-e) high-resolution XPS spectra of Cu 2p, C 1s, O 1s and N 1s of Cu-Cu$_2$O/NC-700 nanocomposite, respectively; (f) ICP-OES analysis results showing Cu weight % ratio (%).
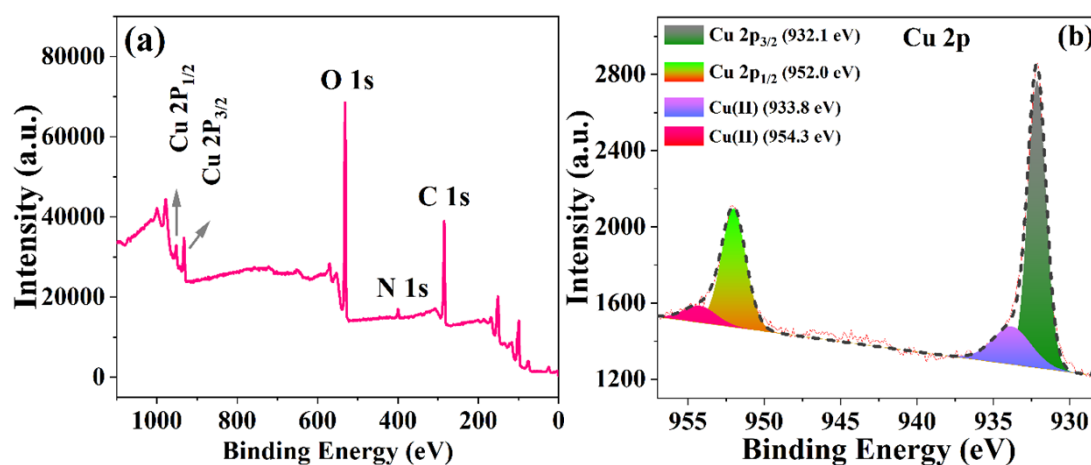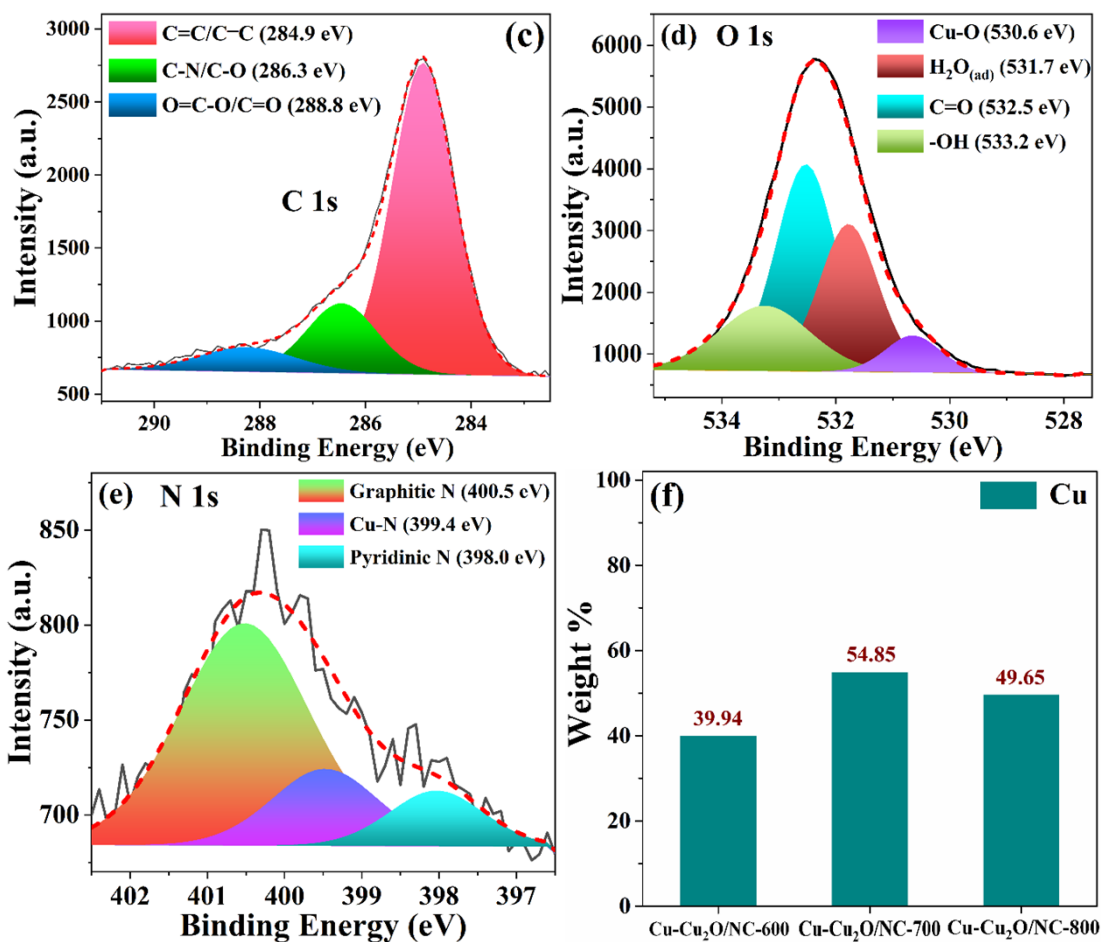
**12. Figure S7.** (a) XRD pattern after 6 h electrolysis at -0.91 V and (b) histogram of particle size distribution for Cu-Cu$_2$O@CC heterostructures; SEM images of Cu(PyDC)(H$_2$O) MOF on carbon cloth (c) before electrolysis, (d) after 5 minutes electrolysis at -0.91 V, (e-g) after 30 minutes of electrolysis at -0.71 V, -0.91 V and -1.11 V, respectively.
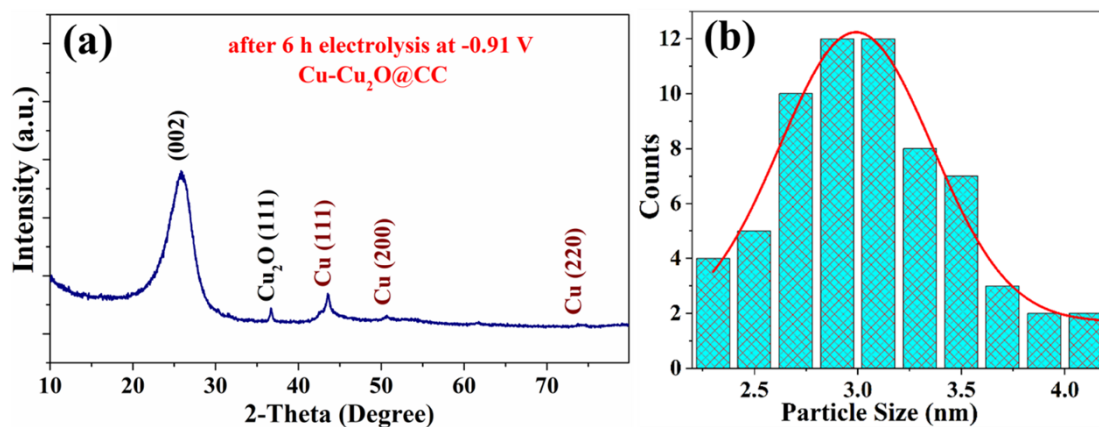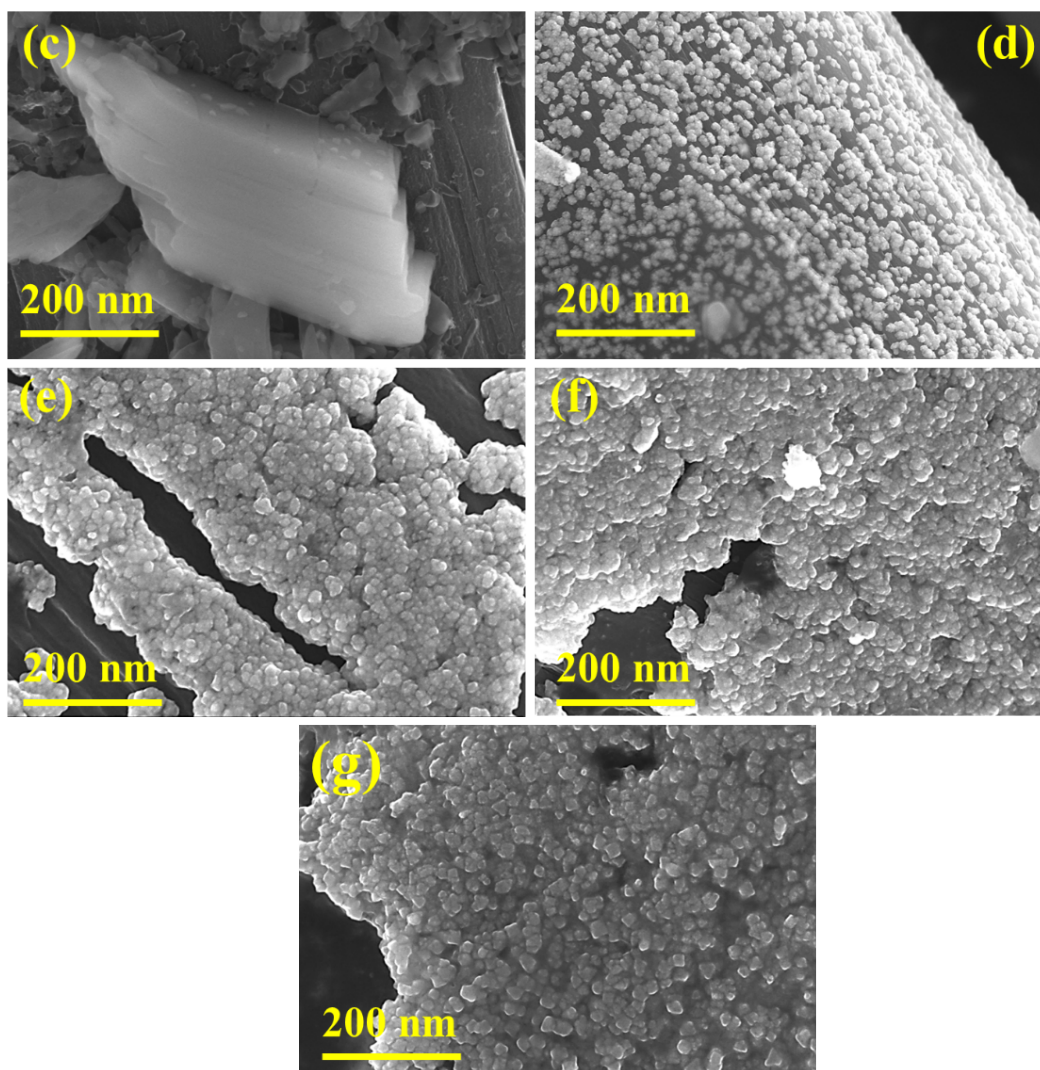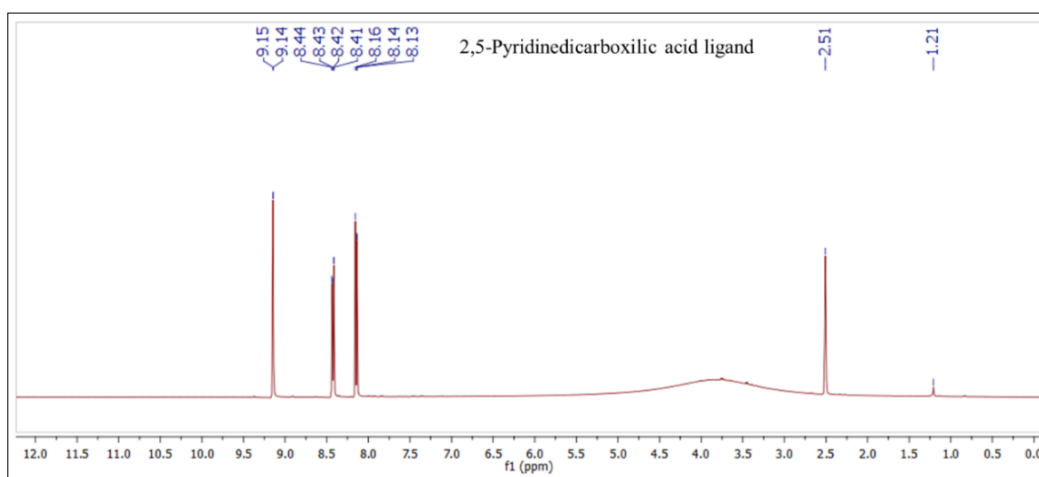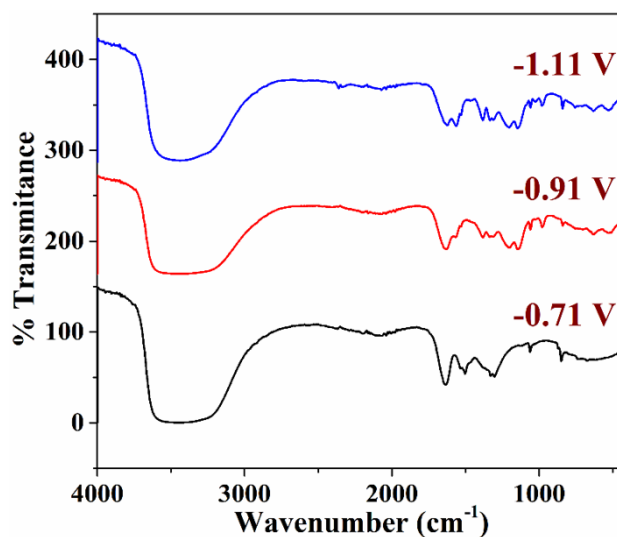
**13. Figure S8.** XPS (a) survey spectra and (b) high-resolution XPS spectra of Cu 2p for 0.5 h $CO_2$ electrolyzed Cu-$Cu_2$O@CC catalysts.
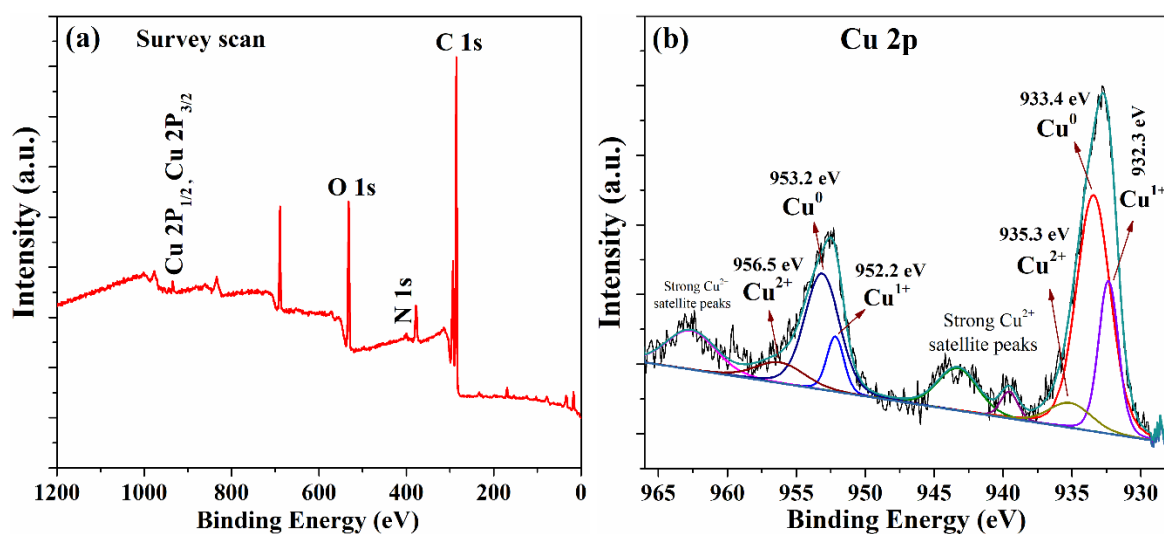

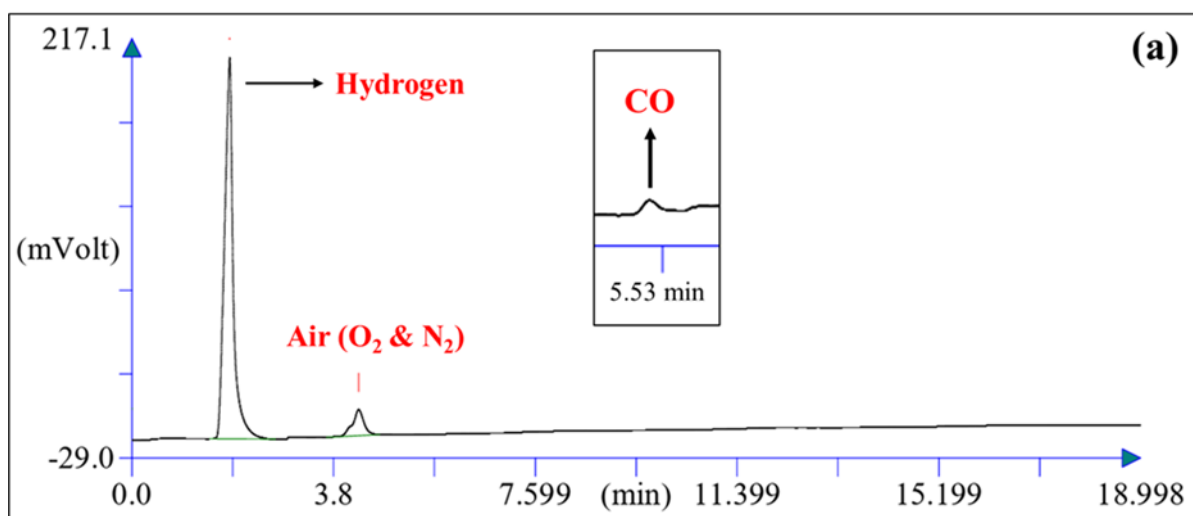
**14. Figure S9.** $^1$H-NMR for 2,5-Pyridinedicarboxilic acid.

**15. Figure S10.** ATR-IR spectra of Cu(PyDC)(H$_2$O) MOF after 30 minutes electrolysis.



**16. Figure S11.** $^1$H NMR spectra and GC data for electrochemical CO$_2$RR products.
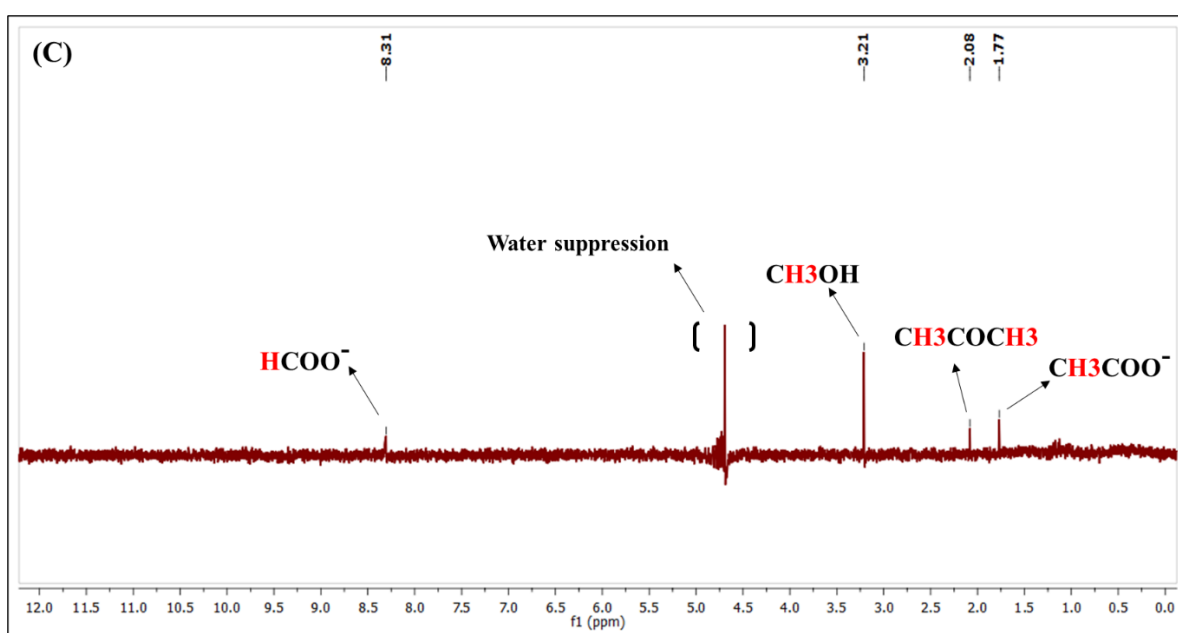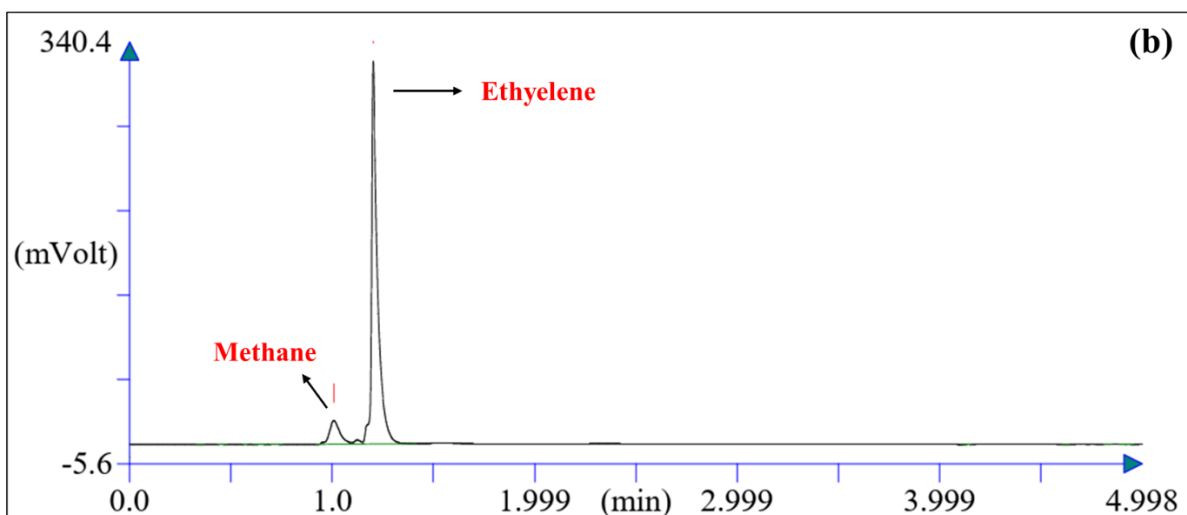
**17. Figure 12:** LSV curves of (a) Cu-Cu$_2$O/NC-600 and (b) Cu-Cu$_2$O/NC-800 composites in both Ar- and CO$_2$-saturated solutions.

**18. Figure S13.** Fitting equivalent circuit of the impedance spectra for Cu-Cu$_2$O@CC heterostructures and Cu-Cu$_2$O/NC composites.

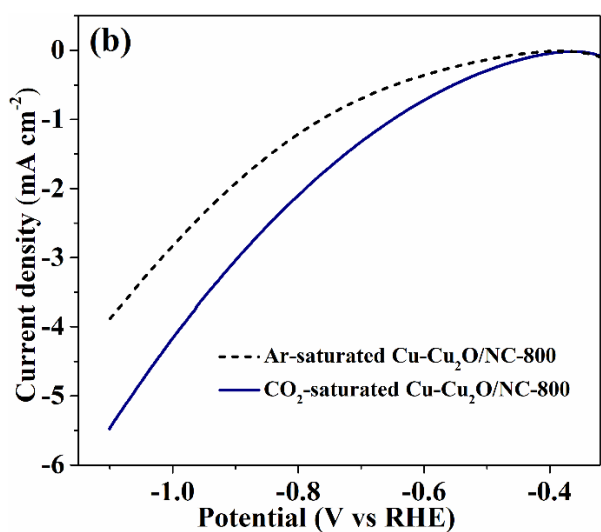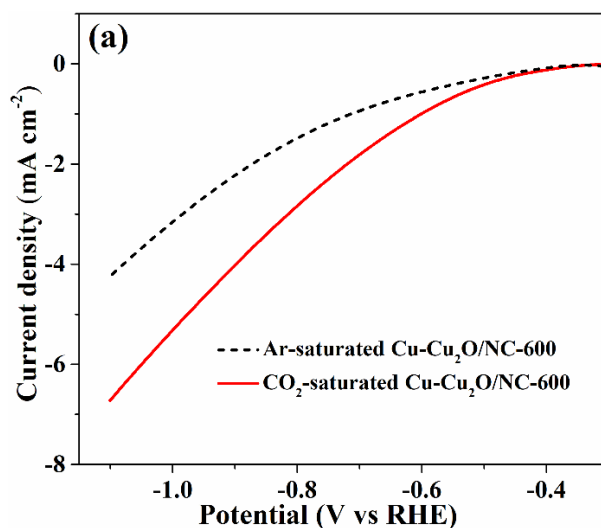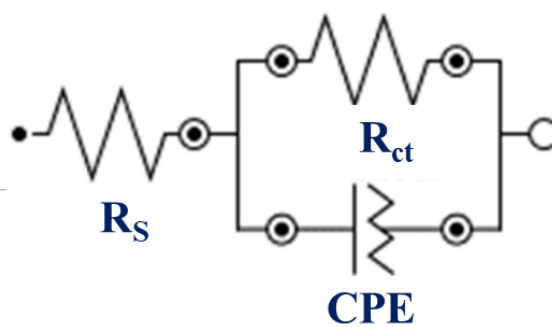**19. Table S3.** Fitting data of impedance spectra for Cu-Cu$_2$O@CC heterostructures and Cu-Cu$_2$O/NC composites.

| Composites | $R_S$ ($\Omega$) | $R_{ct}$ ($\Omega$) |
|---|---|---|
| Cu-Cu$_2$O@CC | 41.7 | 16.5 |
| Cu-Cu$_2$O/NC-600 | 42.2 | 74.0 |
| Cu-Cu$_2$O/NC-700 | 43.8 | 49.0 |
| Cu-Cu$_2$O/NC-800 | 40.5 | 88.5 |

**20. Figure S14.** Faradaic efficiency for (a) Cu-Cu$_2$O/NC-600 and (b) Cu-Cu$_2$O/NC-800 composites.
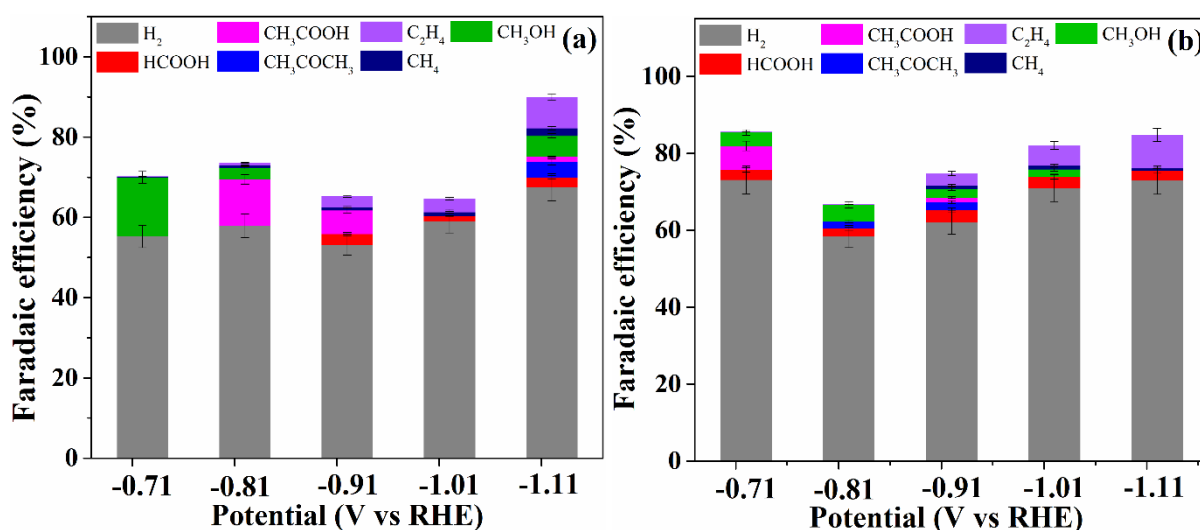


**21. ECSA analysis**

**Figure S15.** CV curves of (a) Cu-Cu$_2$O/NC-600, (b) Cu-Cu$_2$O/NC-700, (c) Cu-Cu$_2$O/NC-800 and (d) Cu-Cu$_2$O@CC heterostructures at different scan rate of 20, 40, 60, 80 and 100 mV S$^{-1}$; (e) plot of current density vs scan rate.
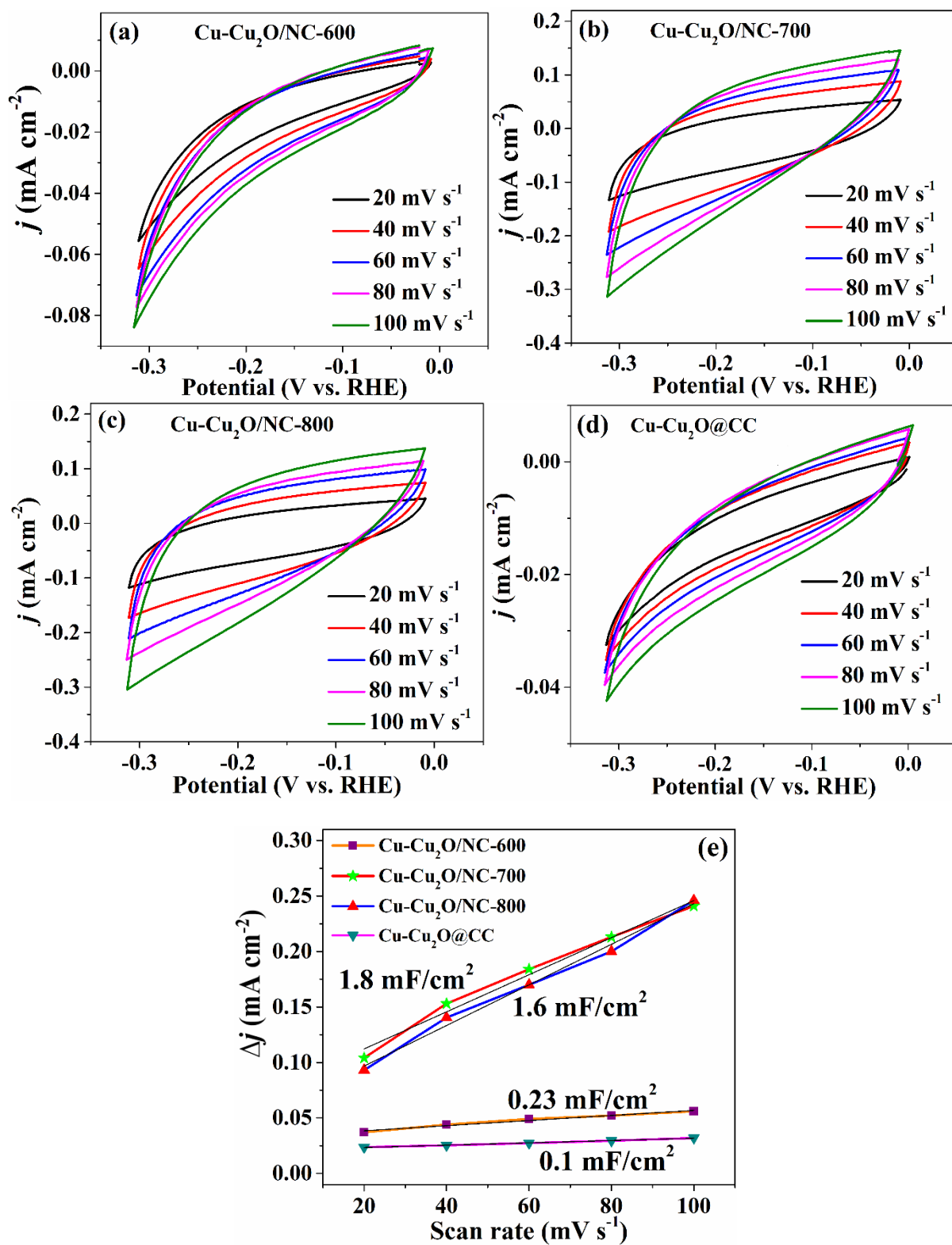
**22. Figure S16.** Stability of the Cu-Cu$_2$O/NC-700 composite at different studied potentials for 6 h of CO$_2$ electroreduction.
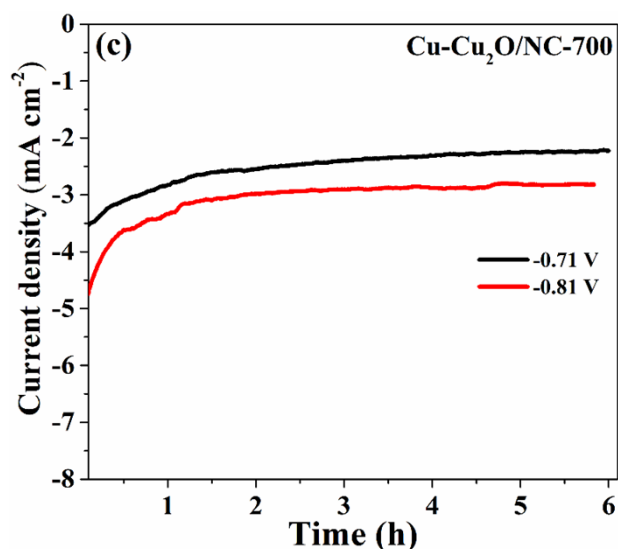
**23. Figure S17.** XPS (a) survey spectra, (b-e) high-resolution XPS spectra of Cu 2p, C 1s, O 1s and N 1s; (f) & (g) are TEM and HR-TEM images of 0.5 h electrolyzed Cu-Cu$_2$O/NC-700 composites, respectively.
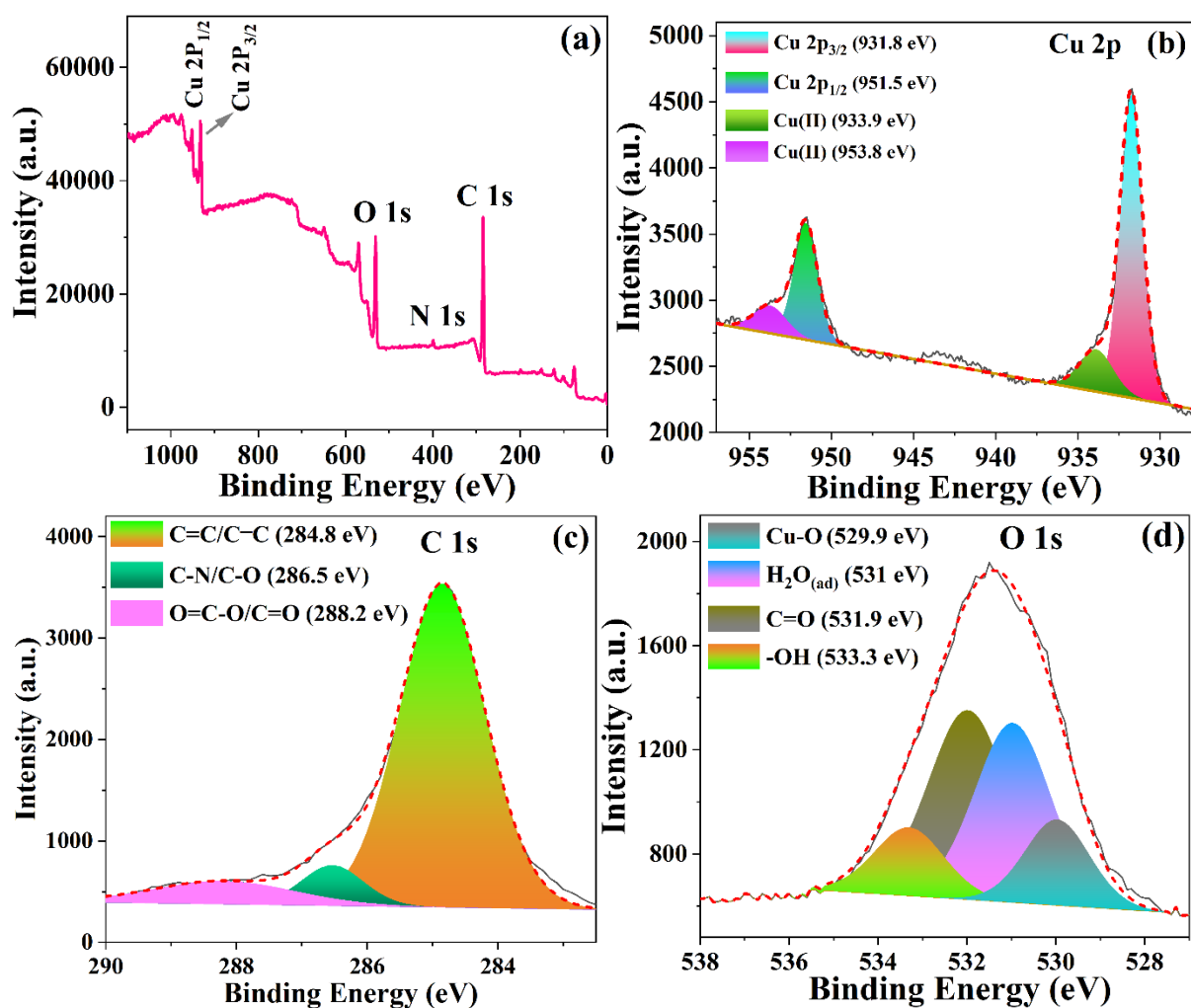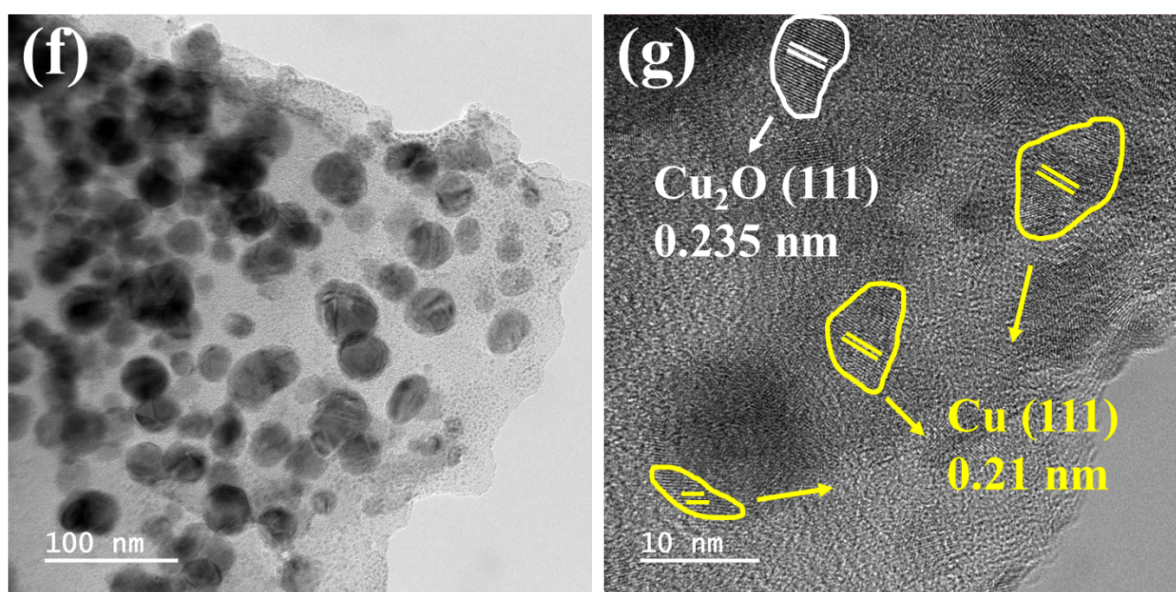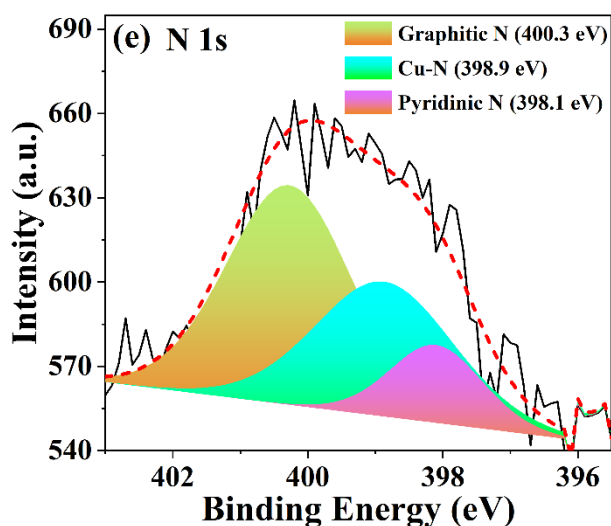
**24. Table S4.** Comparison of recent reported literature for Cu–based electrocatalysts on $CO_2RR$ to $C_2H_4$.

| Catalyst name | Electrolyte | FE of $C_2H_4$ | Applied Potential (vs. RHE) | Ref. |
|---|---|---|---|---|
| Electro-redeposited Cu foil ($Cu_2(OH)_3Cl$ + $Cu_2O$) | 0.1 M $KHCO_3$ | 39% | −1.2 V | *Nat. Catal.* **2018**, 1, 103-110. |
| Anodized-Cu nanowire array | 0.1 M $KHCO_3$ | 38.1% | −1.08 V | *J. Am. Chem. Soc.* **2018**, 140, 8681−8689. |

| | | | | |
|---|---|---|---|---|
| Hydroxide-mediated Cu film | 0.1 M KHCO$_3$ | ~ 31.5% | ~ -1.08 V | *Science* **2018**, 360, 783–787. |
| Cu-ion cycled Cu nanocube on Cu foil (covered with Cu2O) | 0.25 M KHCO$_3$ | 32% | −0.96 V | *Nat. Catal.* **2018**, 1, 111-119. |
| 4H/fcc Au@Cu nanorod | 0.1 M KHCO$_3$ | 35.6% | −1.14 V | *J. Am. Chem. Soc.* **2020**, 142, 12760−12766. |
| Ag@Cu Np | 0.5 M KHCO$_3$ | ~41.3% | −1.2 V | *Inorg. Chem. Front.* **2020**, 7, 2097-2106. |
| **Cu-Cu$_2$O@CC heterostructures** | **0.1 M KHCO$_3$** | **40.53%** | **−1.1 V** | **This work** |

## 25. Computational details

The electronic structure of Cu and Cu$_2$O compounds were carried out using density functional theory within the Perdew-Burke-Ernzerhof [1] generalized gradient approximation (GGA) implemented in Vienna Ab initio Simulation Package [VASP],[2-5] initially the calculation was performed on Cu and Cu$_2$O crystals by taking energy cut-off 500 eV. Further to set up the Cu(111), Cu$_2$O(111), and Cu@Cu$_2$O(111) surface, bulk geometry supercell containing (7x7) for Cu matching with (6x6) supercell of Cu$_2$O was used and optimized with more than 20 Å of vacuum to avoid the interaction between adjacent images for the surface study. Relaxation was carried out till the force on individual atom is less than 0.01 eV/Å. The Brillouin zones were sampled using a K point's mesh with Monkhorst-Pack scheme [6] grid of 6x6x1 for optimization. The adsorption energy to get insight into adsorbability of molecular and intermediate states on Cu(111), Cu$_2$O(111), and Cu@Cu$_2$O(111) surfaces were calculated using below mathematical expression:

$$\Delta E_{ads} = E_{sur+mol} - (E_{sur} + E_{mol})$$

Here $E_{sur+mol}$, $E_{ads}$, and $E_{mol}$ represent the total energy of adsorbate interacting with the substrate, energy of adsorbate, and energy of substrate, respectively. Furthermore, the Gibbs free energy ($\Delta G$) of formation of each step was computed using

$$\Delta G = \Delta E_{ads} + \Delta ZPE - T\Delta S$$

Where $\Delta E_{ads}$, $\Delta ZPE$, and $T\Delta S$ are the adsorption energy, zero-point energy and entropy of the two states before and after the interaction. As we know that ZPE, and $T\Delta S$ values does not depend on the surface so we took these values from the literature.[7, 8]


## 26. DFT simulations

**Figure S18.** The simulation of $CO_2RR$ to $C_2H_4$, and $CH_3OH$ is performed on Cu(111), $Cu_2O(111)$, and $Cu@Cu_2O(111)$ surfaces, reaction process involves step from $CO_2$, COOH, CO, CHO, $C_2H_2O_2$, $CH_2OH$, and $CH_3OH$ [Purple, Red, Blue and Pink ball showing Cu, O, C, and H atoms]
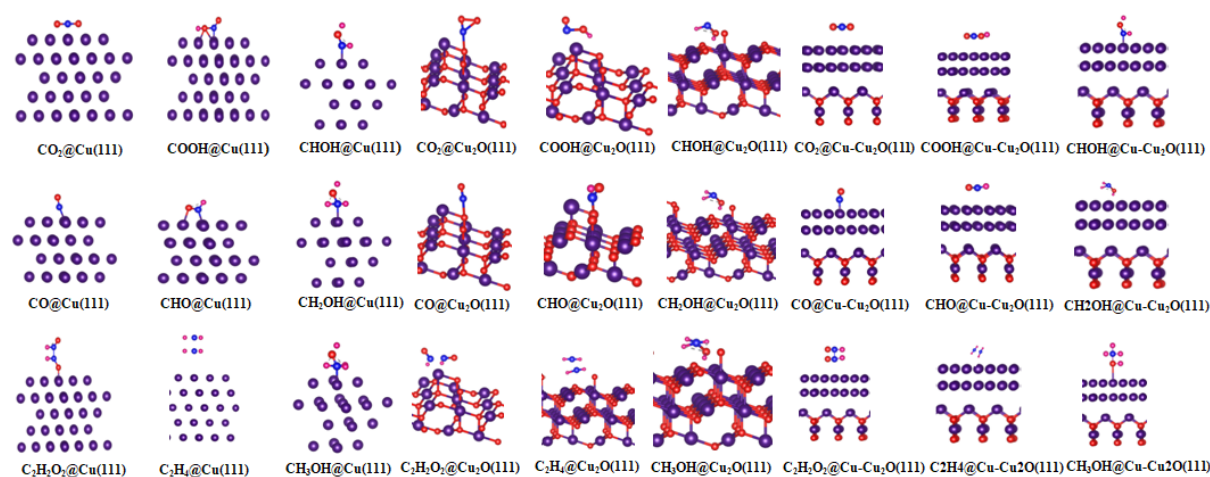


## 27. References

1. Perdew, J. P.; Burke, K.; Ernzerhof, M., Generalized gradient approximation made simple. *Phys. Rev. Lett.* **1996,** 77, 3865.

2.   Kresse, G.; Hafner, J., Ab initio molecular dynamics for liquid metals. *Phys. Rev. B* **1993,** 47, 558.

3.   Kresse, G.; Hafner, J., Ab initio molecular-dynamics simulation of the liquid-metal–amorphous-semiconductor transition in germanium. *Phys. Rev. B* **1994,** 49, 14251.

4.   Kresse, G.; Furthmüller, J., Efficiency of ab-initio total energy calculations for metals and semiconductors using a plane-wave basis set. *Comput. Mater. Sci.* **1996,** 6, 15-50.

5.   Kresse, G.; Furthmüller, J., Efficient iterative schemes for ab initio total-energy calculations using a plane-wave basis set. *Phys. Rev. B* **1996,** 54, 11169.

6.   Monkhorst, H. J.; Pack, J. D., Special points for Brillouin-zone integrations. *Phys. Rev. B* **1976,** 13, 5188.

7.   Gao, S.-T.; Xiang, S.-Q.; Shi, J.-L.; Zhang, W.; Zhao, L.-B., Theoretical understanding of the electrochemical reaction barrier: a kinetic study of $CO_2$ reduction reaction on copper electrodes. *Phys. Chem. Chem. Phys.* **2020,** 22, 9607-9615.

8.   Rahal, M.; Hilali, M.; El Hammadi, A.; El Mouhtadi, M.; El Hajbi, A., Calculation of vibrational zero-point energy. *J. Mol. Struct.* **2001,** 572, 73-80.